JOURNAL OF AIRCRAFT
Vol. 35, No. 4, July–August 1998

Wind-Tunnel Aerodynamics in Rotary Tests of Combat Aircraft Models

Lars E. Ericsson*
Mountain View, California 94040
and
Martin E. Beyers†
Institute for Aerospace Research, Ottawa, Ontario K1A 0R6, Canada

To predict the full-scale aerodynamics of a combat aircraft performing high-alpha maneuvers requires the combined usage of experimental and theoretical tools. The preferred experimental tool is the rotary rig because it provides simulation of one important component of advanced maneuvers, i.e., the velocity vector roll. The present paper analyzes the results obtained in the recently completed investigation by AGARD FDP Working Group 16. Anomalous results are obtained when attempting to simulate high-Reynolds-number rotary characteristics in subscale tests using boundary-layer trips alone or in combination with forebody strakes.

Nomenclature

b = wingspan
d = maximum body diameter
l = rolling moment, coefficient $C_l = l/(\rho_\infty U_\infty^2/2)Sb$
n = yawing moment, coefficient $C_n = n/(\rho_\infty U_\infty^2/2)Sb$
Re = Reynolds number based on d and freestream conditions
S = reference area, projected wing area
t = time
U = horizontal velocity
x = axial body-fixed coordinate
Y = side force: coefficient $C_Y = Y/(\rho_\infty U_\infty^2/2)S$
α = angle of attack
α_S = sting crank angle
Δ = amplitude
θ_A = apex half-angle
ρ = air density
σ = inclination of the roll axis
ς = azimuth
ς_m = azimuth of stagnation point on coning model
ς_t = azimuth of boundary-layer trip
ϕ = roll angle
ψ = coning angle
Ω = dimensionless coning rate, $\omega b/2U_\infty$
ω = coning rate, rad/s

Subscripts
A = apex
CG = center of gravity or rotation center
cr = critical
LS = laminar separation
S = sting
TS = turbulent separation
t = transition trip
WR = wing rock
∞ = freestream conditions

Differential Symbols
$C_{nr} = \partial C_n/\partial(rb/2U_\infty)$
$C_{n\beta} = \partial C_n/\partial\beta$
$C_{n\dot{\beta}} = \partial C_n/\partial(\dot{\beta}b/2U_\infty)$
$r = \partial\psi/\partial t$

Presented as Paper 97-0729 at the AIAA 35th Aerospace Sciences Meeting, Reno, NV, Jan. 6–9, 1997; received Feb. 1, 1997; revision received June 26, 1997; accepted for publication Dec. 12, 1997.

*Engineering Consultant. Fellow AIAA.
†Head Aircraft Aerodynamics Group, Aerodynamics Laboratory. Senior Member AIAA.

Introduction

STEADILY increasing performance demands expose present-day combat aircraft to unsteady flow fields that generate highly nonlinear aerodynamics with strong coupling between lateral and longitudinal degrees of freedom. The complex vehicle dynamics are caused by flow separation effects of various types that have largely eluded theoretical descriptions and, therefore, are placing great demands on dynamic testing capabilities.[1] One very important experimental tool for obtaining the needed information about nonplanar motion effects is the rotary rig. A prerequisite for the successful use of rotary-rig test results is a thorough understanding of how the aerodynamic environment in the wind tunnel differs from that in full-scale flight. The present paper addresses the problem of accounting for the often large difference in Reynolds number between subscale tests and full-scale flight. The strong coupling occurring between boundary-layer transition and vehicle motion can cause the subscale test results to be very misleading. This is particularly true in cases where flow separation occurs in combination with boundary-layer transition.[2] If the flow physics are well understood it is sometimes possible to predict the full-scale vehicle dynamics through analytic extrapolation.[3–5] The scaling problems are discussed in the context of the effects of different forebody modifications used in the tests of the AGARD WG16 model of a representative combat aircraft configuration. The basic model was tested with and without boundary-layer trips and/or forebody strakes.[6]

Effects of Boundary-Layer Trips

It has been common practice to use boundary-layer trips on subscale models in an attempt to simulate full-scale flow conditions. This method has, however, very limited success when the aerodynamic characteristics are dominated by the effects of separated flow, as in the case of the WG16 model[6] (Fig. 1). Figure 2 shows that not only are the body-alone results de-

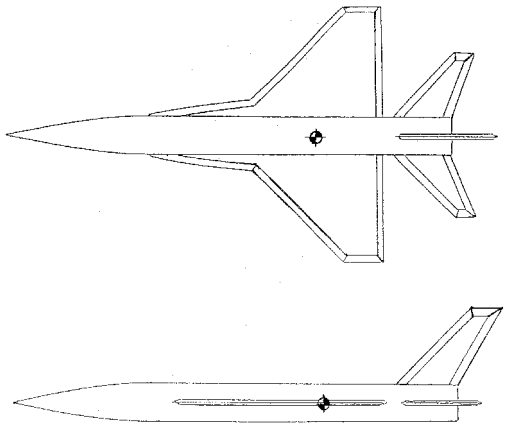

Fig. 1 AGARD WG16 generic combat aircraft model.[6]

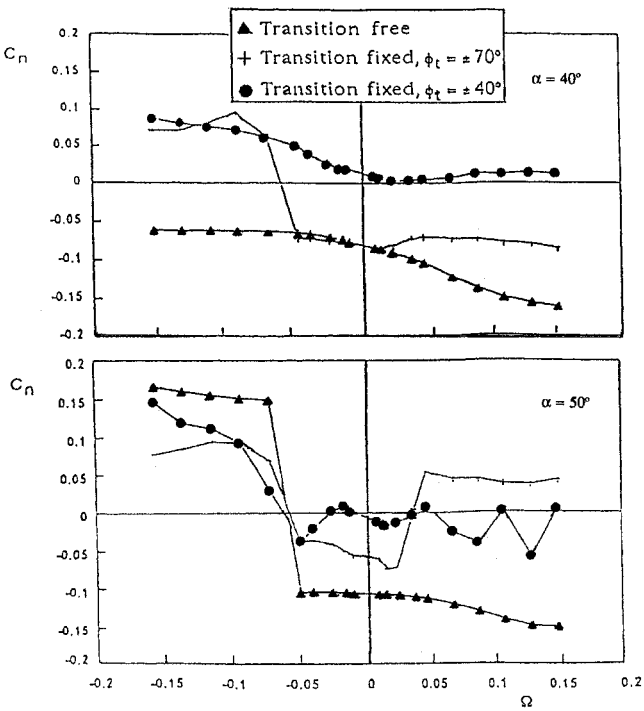

Fig. 2 Effect of boundary-layer trips on body alone for $\alpha_S = 60$ deg.[6]

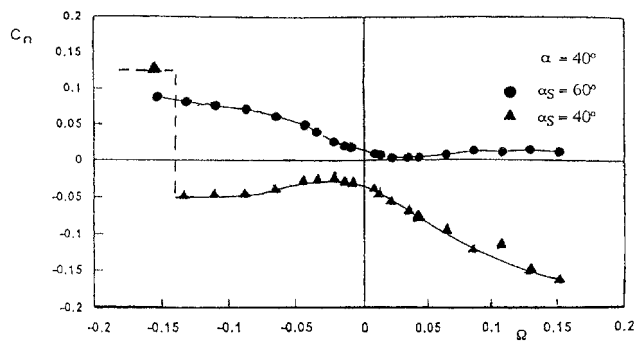

Fig. 3 Effect of α_S at $\alpha = 40$ deg on body alone for $\varphi_t = \pm 40$ deg.[6]

pendent upon the trips, but also the support interference, which has been shown to be large in rotary-rig tests,[7–9] depends strongly on whether transition is free or fixed and also upon the location of the grit strips when used. The large effect of different sting crank angles, $\alpha_S = 60$ deg vs $\alpha_S = 40$ deg at $\alpha = 40$ deg for body-alone with trips at $s_t = \pm 40$ deg (Fig. 3), is similar to that observed previously.[10] The results for $\alpha = 40$ deg in Fig. 4 for the complete model show that the use of trips changes the effect of the nose strakes (Fig. 5), even changing the sign of the rolling moment for the complete configuration. The different effects of trips and/or strakes for positive and negative coning rates in Figs. 2 and 4 reveal the strong coupling between the viscous flow conditions, as affected by the grit strips used, and the prevailing ground facility interference.[2,7–11] Figure 4 shows that at $\alpha = 40$ deg the presence of the trips influenced C_Y greatly for $\Omega < -0.1$ and $\Omega > 0.05$, but they did not affect the C_n characteristics. This indicates that the forebody vortices have a significant effect on downstream wing-body surfaces, as is verified by the C_l characteristics.

Considering the lessons learned when attempting to control asymmetric crossflow separation by the use of body trips in the case of static tests,[12] one could have expected that it would be very difficult to achieve the desired results with tripping devices in the present coning tests. Even though they used distributed roughness, Hall and Banks[13] concluded that "the sectional side forces produced by the gritting patterns were 50% larger than the grit-free high Reynolds number data." The largest difficulty is to determine to what extent asymmetric

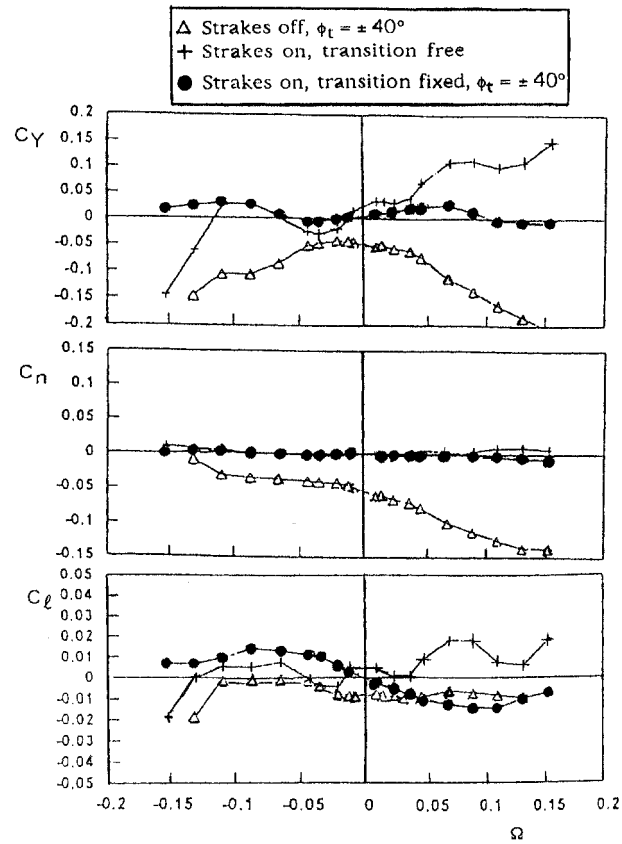

Fig. 4 Effect of nose strakes and trips on complete model ($\alpha = \alpha_S = 40$ deg).[6]

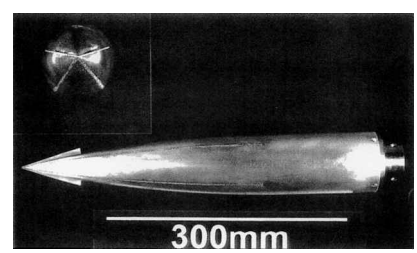

Fig. 5 AGARD WG16 model with nose strakes and grit strips at $\varphi_t = \pm 40$ deg.[6]

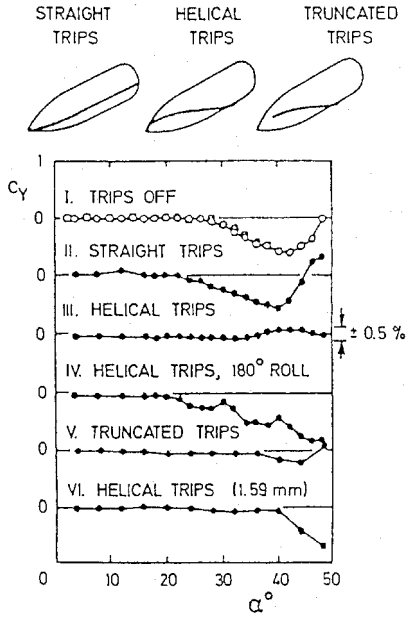

Fig. 6 Effect of helical and straight body trips on side force of ogive–cylinder body.[14]

boundary-layer transition in the near-tip region affects the crossflow separation and associated vortex shedding.[12] The tests performed with helical trips by Rao[14] illustrate the difficulties involved (Fig. 6). The helical trips were found to be effective in reducing the side force, but the usually effective straight trips were not. Whereas a nose strake generates its own crossflow separation and associated vortex geometry, the body trip acts only via its local action on the boundary-layer development over the forebody. Its location relative to the natural separation line is crucial. The flow physics causing the different effects of the tested trips shown in Fig. 6 are described in Ref. 15.

The variation of side-force characteristics in Fig. 6 gives ample warning that one should expect the grit strips on the WG16 model to produce local tripping effects that vary along the length of the forebody. Adding this to the effect of coning rate, Reynolds number, wind-tunnel turbulence, and ground facility interference, it became clear how difficult it would be to simulate high-Reynolds-number characteristics in the test of the WG16 model.

Coning Characteristics

The simulation of unsteady turbulent crossflow conditions by the use of boundary-layer transition trips is extremely difficult. Full simulation in dynamic tests with subscale aircraft models is possible only if the full-scale Reynolds number can be simulated by the use of a pressurized test section or a cryogenic wind tunnel.[2] Of course, in the present case of interest the incident flow conditions are stationary rather than nonstationary, and one would expect the simulation problem to be rather benign. However, this turns out not to be the case.

The rotation of the flow stagnation point as a result of the coning-induced lateral velocity component at x is

$$\phi_m = \tan^{-1}[2(x_{CG}/b - x/b)\Omega] \qquad (1)$$

For the maximum rate tested, $\Omega = 0.15$, Eq. (1) gives $\phi_m = 19.4$ deg at the nose tip and $\phi_m = 10.1$ deg at the apex of the leading-edge extension (LEX). In the analysis that follows the more representative rate $\Omega = 0.1$ is used for the cross section translating in the starboard direction, giving $\phi_m = 11.6$ deg for the crossflow geometry immediately aft of the nose strakes.

Figure 7a illustrates the crossflow characteristics existing for turbulent crossflow conditions. The moving-wall effects in the stagnation region will cause the flow separation to be delayed on the advancing side and promoted on the receding side,[16,17] generating a prospin force as indicated. Figure 7b shows that a similar separation geometry exists for purely laminar flow conditions, also resulting in a prospin force as has been demonstrated[18,19] (Fig. 8). Experimental results for a fighter aircraft model[20] (Fig. 9) showed that body-alone aerodynamics could in that case represent the essential high-alpha $C_m(\Omega)$ characteristics of the complete aircraft. In contrast, the WG16 model has LEX surfaces extending forward all the way to the base of the slender forebody. As will be shown later, the LEX-induced upwash dominates over the moving-wall effects, reversing the $C_n(\Omega)$ trend from proconing to anticoning. However, many existing aircraft, such as the F-14 with its flat-spin tendency, discussed in Ref. 21, have geometries similar to that shown in Fig. 9, making this a case of current interest.

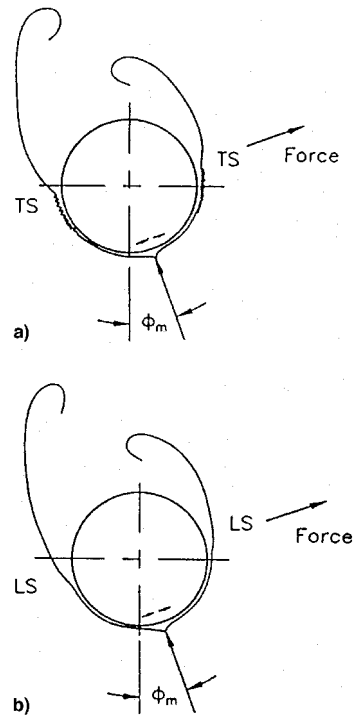

Fig. 7 Conceptual crossflow characteristics of translating circular cross section: a) turbulent and b) laminar crossflows.

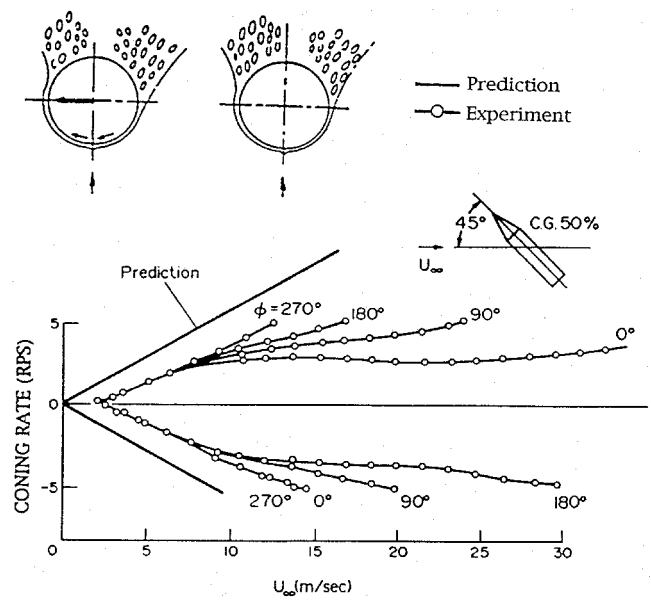

Fig. 8 Coning characteristics of a pointed cone–cylinder body.

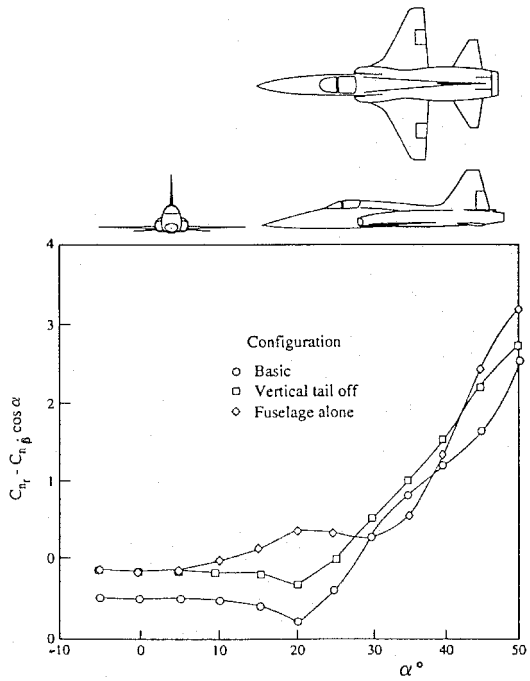

Fig. 9 Yaw damping of fighter aircraft model.[20]

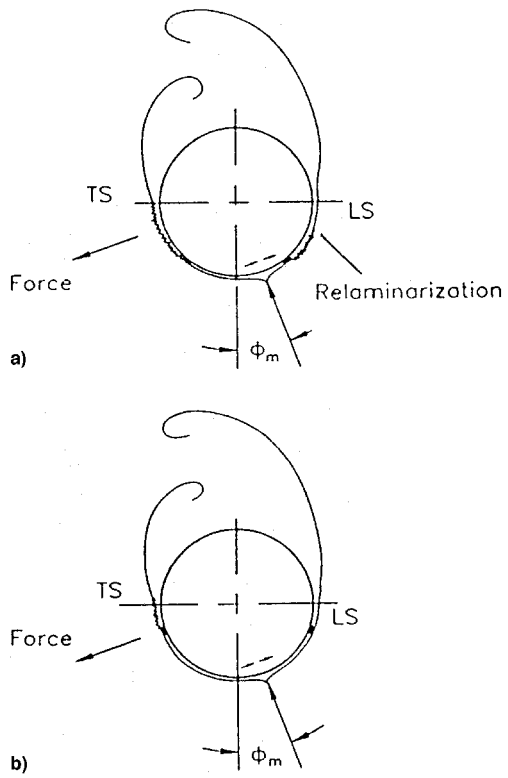

Fig. 10 Conceptual crossflow characteristics of translating circular cross section for laminar flow conditions. Trips at φ_t = a) ±40 deg and b) ±70 deg.

In contrast to the crossflow characteristics for a clean forebody (Fig. 7), the trips at $\varsigma_t = \pm 40$ deg at subcritical flow conditions will generate the crossflow characteristics shown in Fig. 10a. On the advancing side the trip at $\varsigma_t = 40$ deg is close to the stagnation point and there is a long run of favorable pressure gradient after the trip. Thus, even if the trip caused a transition to turbulent flow, relaminarization is likely to occur before flow separation. [This was indeed the case at $Re = 0.205 \times 10^6$ (Ref. 22).] At critical flow conditions, $Re = 0.3 \times 10^6$ in Figs. 2 and 4, relaminarization is likely to have occurred on the advancing side of the forward portion of the nose. In contrast, on the receding side the trip is farther away from the stagnation point and the trip could cause a transition to turbulent flow conditions before separation, resulting in a substantial delay of the crossflow separation compared to the other side. The net result would be the generation of an antispin force, as illustrated in Fig. 10a, contrary to the prospin force expected for turbulent flow (Fig. 7a). For the trips at $\varsigma_t = \pm 70$ deg (Fig. 10b) it is very unlikely that the turbulent flow has time to develop on the advancing side. It is even possible that the trip could promote laminar flow separation on this side. Thus, it is likely that the trips at $\varsigma_t = \pm 70$ deg would also generate antispin crossflow characteristics.

The detailed crossflow characteristics in Fig. 10 depend on both the Reynolds number and the coning rate. Figure 2 shows that at $\alpha = 40$ and 50 deg discontinuous changes of the steady-state $C_n(\Omega)$ take place at certain values of the coning rate, indicating the possible existence of threshold values that the rate has to exceed to overcome the inertia of the bistable flow condition, which in turn is influenced by support interference, allowing the flow geometries sketched in Fig. 10 to be established. The existence of such a threshold is investigated in Ref.

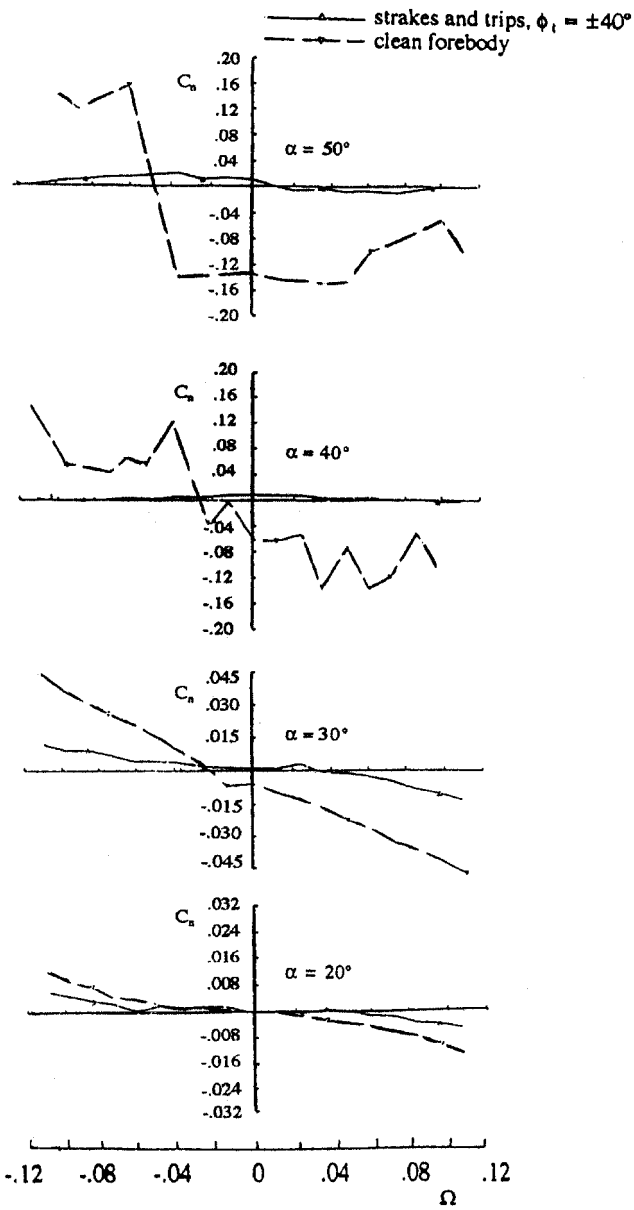

Fig. 11 Effect of strakes and trips at $Re = 0.205 \times 10^6$ on $C_n(\Omega)$ characteristics for the AGARD generic fighter model.[6,24]

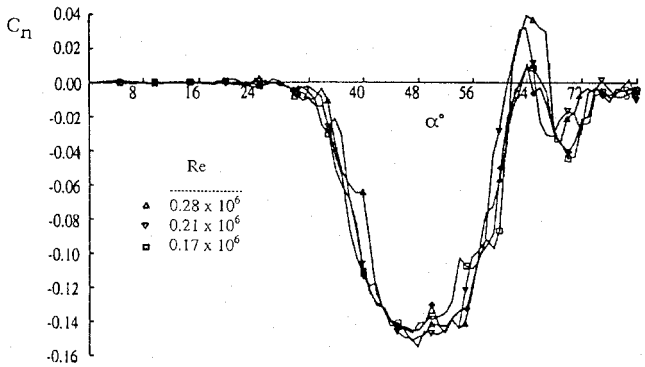

Fig. 12 Effect of Reynolds number on static yawing moment characteristics of the clean basic configuration (BC).[6]

11. From the experimental results for body alone at $\alpha = 40$ deg in Fig. 2, it appears that $\Omega = -0.05$ was such a threshold value. Thus, both trip locations generated antispin forces at $\Omega < -0.05$, in agreement with the flow sketches in Figs. 10a and 10b, respectively. At $\alpha = 50$ deg a second cell of asymmetric crossflow separation[12] is established aft of the nose tip at $\alpha \geq 46$ deg (Ref. 23).

Experimental results at $Re = 0.205 \times 10^6$ for the basic configuration without trips[6] (clean forebody in Fig. 11) show $C_n(\Omega)$ characteristics with antispin tendencies that increase with α up through $\alpha = 30$ deg. At $\alpha = 40$ and 50 deg this trend becomes very erratic. (Note the changing ordinate scale between different angles of attack.) It is no surprise that the stabilizing data trend $C_n(\Omega)$ is strongest at $\alpha = 30$ deg.[24] As $\theta_A = 14.25$ deg, the static asymmetry[12] starts at $\alpha > 28.5$ deg as expected (Fig. 12). Consequently, at $\alpha > 30$ deg the effect of the coning rate is decreased greatly.[24] At $\alpha = 50$ deg the microasymmetry effect apparently dominates at $|\Omega| \geq -0.08$, as the $|C_n|$ value agrees with the static results in Fig. 12. The rate Ω at which the discontinuity occurs is influenced by support interference. The aerodynamics of the clean configuration are analyzed further in Ref. 11. Throughout the α range the effect of adding the nose strakes (strakes and tips in Fig. 11) was to greatly reduce the magnitude of the measured yawing moment.

Low-*Re* Test Results

The test Reynolds number for the results in Fig. 11, $Re = 0.205 \times 10^6$, would be expected to produce laminar crossflow conditions, particularly when considering that this is the upper *Re* limit for the crossflow on the slender nose. At the time of these tests the authors knew of only one flow mechanism that could establish the measured anticoning data trend, i.e., moving-wall effects at critical crossflow conditions.[16] One possibility was, of course, that tunnel turbulence could have caused the crossflow conditions to become of the critical type even at this low-Reynolds number. In that case the upstream moving-wall effects would promote transition,[2,16] resulting in the crossflow geometry sketched in Fig. 13. This would have produced antispin forces on the forebody, in agreement with the experimental results in Fig. 11. However, the test covered a large enough Reynolds-number range to determine whether or not the crossflow conditions could have been in or near the critical range. Thus, Fig. 12 can show conclusively that the experimental results for $Re = 0.205 \times 10^6$ in Fig. 11 were well below the critical range. Otherwise, large variations of the side force and yawing moment would have been observed for the Reynolds-number range tested.[12] Thus, in the absence of LEX surfaces, the crossflow geometry should have been that shown in Fig. 7b giving a prospin rather than an antispin moment.

The water-tunnel flow visualization results at $\alpha = 40$ deg in Fig. 14a for the complete no-strake configuration show the existence of symmetric forebody vortices for $\Omega = 0$. This is in agreement with past experience that, at the low-Reynolds numbers of water-tunnel tests, the onset of asymmetric crossflow

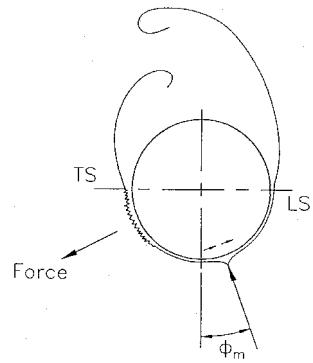

Fig. 13 Conceptual crossflow geometry of translating circular cross section at critical flow conditions.

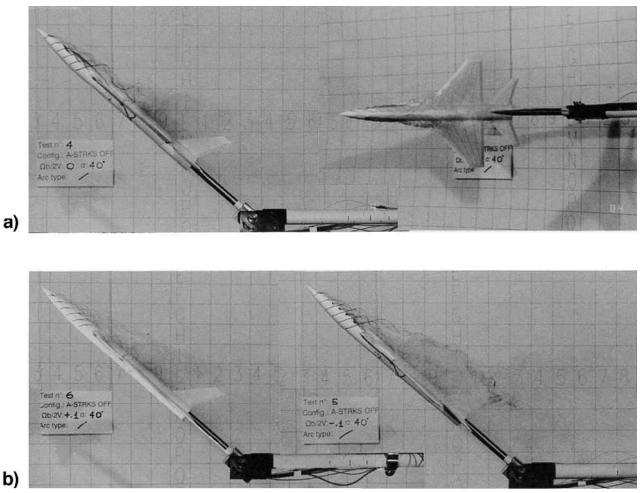

Fig. 14 Flow visualization of basic AGARD WG16 model at $\alpha = 40$ deg.[6] Ω = a) 0 and b) ± 0.10.

separation is delayed relative to its occurrence in wind-tunnel tests. In Ref. 22 it is shown that the results in Fig. 14a are consistent with those in Fig. 12. The antispin characteristics in Fig. 11 still must be explained.

Because the crossflow conditions in Fig. 11 are laminar, the crossflow separation would look similar to that shown in Fig. 7b, producing a prospin yawing moment. This is certainly true for body alone (Fig. 8) and for the fighter aircraft model in Fig. 9. Why, then, is the WG16 model producing antispin $C_n(\Omega)$ characteristics (Fig. 11)? One difference between the aircraft geometries producing the results in Figs. 9 and 11 is the presence of the LEXs on the WG16 model (Fig. 1). The wing rock observed in tests with another generic aircraft model[25] (Fig. 15) was caused by moving-wall effects generated by a rolling motion rather than coning.[26] Moving the wing forward to the base of the slender nose eliminated the wing rock existing for the wing in the aft position[25] (Fig. 15). As described in Ref. 27, the symmetric wing upwash over the forebody was so large in the forward position that the critical flow conditions generating asymmetric crossflow separation, existing at $\sigma = 30$ deg for the aft wing position, could not be established. Likewise, the symmetrizing effect of the LEX-induced upwash at $\Omega = 0$, in spite of the increased effective angle of attack on the forebody, delayed the occurrence of asymmetric crossflow separation from the expected value,[12] $\alpha = 2\theta_A = 28.5$ deg to $\alpha > 35$ deg (see Fig. 12 and Ref. 11). Oscillatory-motion and support-interference effects may also have played a role. As a consequence of this dominance, the coning-induced difference in upwash on downwind and upwind sides of the forebody is able to overpower the coning-induced moving-wall effect in determining the lateral direction of the asymmetric laminar crossflow separation on the forebody.

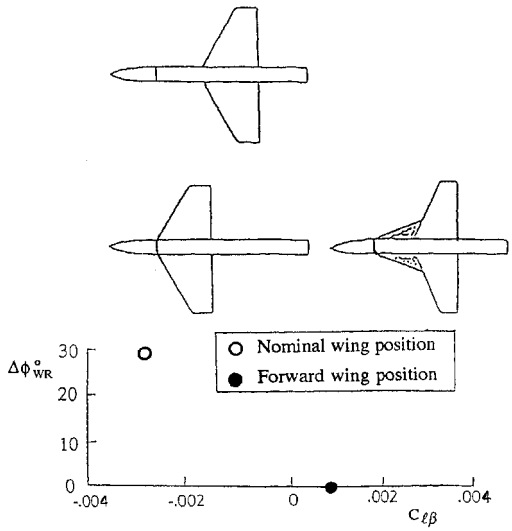

Fig. 15 Effect of wing location on forebody-induced wing rock.[25]

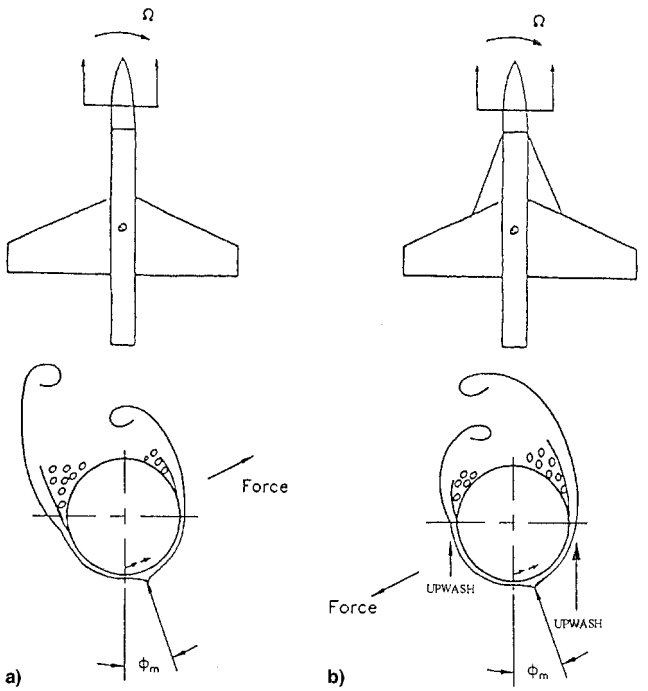

Fig. 16 Conceptual crossflow separation on a coning slender forebody: a) without LEX and b) with LEX.

Figure 16 illustrates the conceptual effect of the LEX-induced upwash on the forebody in the case of a coning motion.[28] Flow visualization results at $\alpha = 39$ deg and $\Omega = 0$ show fully developed leading-edge vortices existing at a cross section close to the LEX-wing juncture (Fig. A4.2.15 in Ref. 22). The coning rate generates a local sideslip distribution that decreases the effective leading-edge sweep of the LEX surfaces on the advancing side and increases it on the receding side. This results in a stronger LEX-induced upwash on the advancing side than that on the receding side, as indicated in Fig. 16b. Assuming that the LEX-induced upwash dominates over the moving-wall effects, as discussed earlier, the crossflow separation and associated vortex shedding on the slender forebody would be affected as seen in Fig. 16. That is, instead of generating a prospin force as in the absence of LEX surfaces (Fig. 16a), the LEX-induced upwash causes the crossflow separation to generate an antispin force on the forebody (Fig. 16b), in agreement with the flow visualization results in Fig. 14. This most likely requires the coning-induced sideslip to

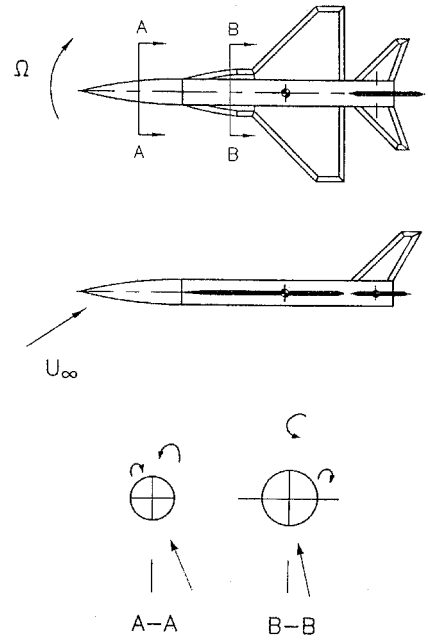

Fig. 17 Conceptual forebody-LEX vortex interaction at $\alpha = 40$ deg and $\Omega > 0$.

exceed a certain threshold value,[11] generated at $|\Omega| > \Omega_{cr}$ ($\Omega_{cr} <$ 0.10 in Fig. 14). The nose strakes eliminated this LEX-induced crossflow asymmetry, resulting in the measured large reduction of the magnitude of the antispin moment (Fig. 11).

Combining the flow sketches in Figs. 10a and 16b, one concludes that the effect of the trips would be to amplify the asymmetry of the crossflow separation and vortex shedding shown in Fig. 16b. Thus, the measured anticoning $C_n(\Omega)$ trend at $\alpha = 40$ deg for strakes-off, $\phi_t = \pm 40$ deg in Fig. 4, is contrary to what it would be for purely laminar or turbulent flow conditions. Strakes eliminated the forebody flow asymmetry and, thereby, the nonzero $C_n(\Omega)$. However, the strakes had no such effect on $C_Y(\Omega)$ or $C_l(\Omega)$, indicating that downstream vortex interactions generate significant loads. One interpretation of the results in Fig. 4 is that the forebody/LEX vortex interaction sketched in Fig. 17 had occurred; i.e., the sidewash induced by the high, lifted-off forebody vortex caused the low, attached forebody vortex to be displaced laterally to interact with the LEX vortex on the opposite side.[11] Apparently, the nose strakes could not eliminate forebody-LEX vortex interaction effects entirely, judging by the $C_Y(\Omega)$ and $C_l(\Omega)$ results in Fig. 4.

Trip Effects on Strake-On Characteristics

At $\alpha > 46$ deg, where the second cell of asymmetric crossflow separation has been established,[23] one can expect the full effect of the trips to also be present for the strake-on configuration.[11] For $\alpha < 46$ deg, the trips could affect the primary crossflow separation for strake-on to change the vortex geometry as shown in Fig. 18. Assuming that the strakes act as forward-facing steps, the nature of the approaching boundary layer, laminar vs turbulent, will affect the extent of the induced crossflow separation and thereby affect the separation-induced forebody vortices. Figure 18a sketches the expected full-scale flow geometry for incident turbulent flow conditions, and Fig. 18b illustrates the crossflow geometry for incident laminar flow conditions in the presence of trips. The adverse moving-wall effect on the receding side reinforces the trip effect, causing turbulent crossflow separation, whereas on the advancing side the downstream moving-wall effect is likely to prevent the trip from establishing turbulent flow conditions. That is, even at $\alpha < 46$ deg the trips will not be able to provide full simulation of the full-scale crossflow conditions for the strake-

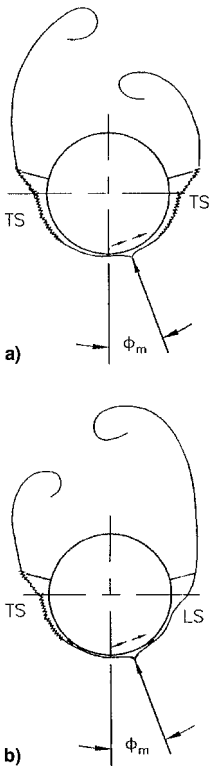

Fig. 18 Conceptual crossflow characteristics of translating circular cross section with strakes: a) turbulent incident crossflow without trips and b) laminar incident crossflow with trips.

on configuration. A similar situation will result also in the absence of strakes at moderately high angles of attack, $\theta_A < \alpha < 2\theta_A$ ($\theta_A = 14.25$ deg), when the forebody vortices are symmetric at $\Omega = 0$ (Ref. 12). As Fig. 18 indicates and the strake-on $C_n(\Omega)$ characteristics in Fig. 4 confirm, the trip effect on the local forebody side force is probably insignificant. However, the difference in forebody vortex geometry apparently had a significant effect on $C_l(\Omega)$ characteristics through the forebody-LEX vortex interaction, determined by the crossflow characteristics on the aft forebody[11] (Fig. 17).

The use of distributed roughness in lieu of boundary-layer trips avoids the situation sketched in Fig. 10b, where the trip may initiate the laminar crossflow separation. However, full simulation of full-scale flow conditions would require the circumferential roughness distributions in the forebody cross sections to be changed every time the crossflow stagnation point moved in response to a change of the coning rate, as the scaled roughness height varies with the local boundary-layer thickness. As suggested by one reviewer, by testing a number of grit patterns over the full range of coning rates, a database could possibly be established that would make it possible to extrapolate analytically[3,4] from the test results to define the rotary rig data that would exist at full-scale Reynolds numbers. However, it should also be emphasized that the results obtained in the absence of trips (clean forebody in Fig. 11) provide an approximation of the full-scale characteristics of combat aircraft when the kinematic effect of the LEX-induced upwash overpowers the viscous moving-wall effect, as was discussed in connection with Fig. 16.

Conclusions

Fluid/motion coupling and ground facility interference effects make the high-alpha wind-tunnel aerodynamics of a subscale model more complex than those of the full-scale aircraft in flight. A thorough understanding of the tunnel aerodynamics is a necessary and often sufficient condition for successful prediction of the full-scale free-flight characteristics. The present analysis has shown the following:

1) For aircraft with clean, axisymmetric forebodies, with and without LEXs, conventional rotary tests performed at laminar flow conditions can provide the qualitative full-scale free-flight characteristics.

2) In the presence of significant LEX/wing-induced upwash effects the forebody crossflow characteristics become far less sensitive to viscous fluid/motion coupling effects.

3) For all practical purposes it is impossible to fully simulate the conditions at a higher Reynolds number by using boundary-layer trips in rotary tests. However, systematic tests with different grit patterns over the full range of coning rates could provide the database needed for analytic extrapolation to full-scale Reynolds-number conditions.

Acknowledgments

This paper benefitted from the comments made by members of AGARD FDP WG16 in regard to the authors' contributions to the final report. The authors also gratefully acknowledge the contributions of Hui Juan Cai, in the flowfield analysis and computer graphics, and Roxanne Preseault in computer graphics and word processing.

References

[1]Orlik-Rückemann, K. J., "Dynamic Stability Testing of Aircraft—Needs Versus Capabilities," *Progress in Aerospace Sciences*, Vol. 16, No. 4, 1975, pp. 431–447.

[2]Ericsson, L. E., "Effects of Transition on Wind Tunnel Simulation of Vehicle Dynamics," *Progress in Aerospace Sciences*, Vol. 27, 1990, pp. 121–144.

[3]Ericsson, L. E., and Reding, J. P., "Dynamic Simulation Through Analytic Extrapolation," *Journal of Spacecraft and Rockets*, Vol. 19, No. 2, 1982, pp. 160–166.

[4]Ericsson, L. E., and Reding, J. P., "Analytic Extrapolation to Full-Scale Aircraft Aerodynamics," *Journal of Aircraft*, Vol. 21, No. 3, 1984, pp. 222–224.

[5]Beyers, M. E., and Ericsson, L. E., "Viscous-Flow/Vehicle-Motion Coupling," *Fluid Dynamics of Rotary Flows, Rotary Balance Testing for Aircraft Dynamics*, AGARD-AR-265, Dec. 1990, pp. 164–167, 183–187, Chap. 8.

[6]Anon., "Cooperative Programme on Dynamic Wind Tunnel Experiments for Maneuvering Aircraft," AGARD-AR-305, Oct. 1996.

[7]Beyers, M. E., and Ericsson, L. E., "Ground Facility Interference on Aircraft Configurations with Separated Flow," *Journal of Aircraft*, Vol. 30, No. 5, 1993, pp. 682–688.

[8]Ericsson, L. E., and Beyers, M. E., "Ground Facility Interference on Slender Vehicle Dynamics," *Journal of Aircraft*, Vol. 33, No. 1, 1996, pp. 117–124.

[9]Ericsson, L. E., "Reflections Regarding Recent Rotary Rig Results," *Journal of Aircraft*, Vol. 24, No. 1, 1987, pp. 25–30.

[10]Ericsson, L. E., and Beyers, M. E., "Special Aerodynamic Considerations," AGARD-AR-265, Dec. 1990, pp. 88–97, Chap. 5.

[11]Beyers, M. E., and Ericsson, L. E., "Extraction of Subscale Free-Flight Aerodynamics from Rotary Tests of Combat Aircraft," AIAA Paper 97-0730, Jan. 1997.

[12]Ericsson, L. E., and Reding, J. P., *Asymmetric Flow Separation and Vortex Shedding on Bodies of Revolution*, Vol. 141, Progress in Astronautics and Aeronautics, AIAA, Washington, DC, 1992, pp. 391–452.

[13]Hall, R. M., and Banks, D. W., "Progress in Developing Gritting Techniques for High Angle of Attack Flows," AIAA Paper 94-0169, Jan. 1994.

[14]Rao, D. M., "Side Force Alleviation on Slender, Pointed Forebodies at High Angles of Attack," *Journal of Aircraft*, Vol. 16, No. 11, 1979, pp. 763–768.

[15]Ericsson, L. E., and Reding, J. P., "Alleviation of Vortex-Induced Asymmetric Loads," *Journal of Spacecraft and Rockets*, Vol. 17, No. 6, 1980, pp. 548–553.

[16]Ericsson, L. E., "Moving Wall Effects in Unsteady Flow," *Journal of Aircraft*, Vol. 25, No. 11, 1988, pp. 977–990.

[17]Ericsson, L. E., *A Critical Look at Dynamic Simulation of Viscous Flow*, CP-386, AGARD, 1985 (Paper 6).

[18]Ericsson, L. E., "Prediction of Slender Body Coning Characteristics," *Journal of Spacecraft and Rockets*, Vol. 28, No. 1, 1991, pp. 43–49.

[19]Yoshinaga, T., Tate, A., and Inoue, K., "Coning Motion of Slender Bodies at High Angles of Attack in Low Speed Flow," AIAA Paper 81-1899, Aug. 1981.

[20]Grafton, S. B., Chambers, J. R., and Coe, P. L., Jr., "Wind Tunnel Free-Flight Investigation of a Model of a Spin Resistant Fighter Configuration," NASA TN D-7716, June 1974.

[21]Ericsson, L. E., and Beyers, M. E., "On the Flat Spin of Axisymmetric Bodies," *Journal of Aircraft*, Vol. 32, No. 6, 1995, pp. 1205–1212.

[22]Beyers, M. E., and Ericsson, L. E., "Aerodynamic Analysis and Interpretation of WG16 Results," AGARD-AR-305, Appendix 4, Oct. 1996.

[23]Cai, H. J., and Beyers, M. E., "Oscillatory Experiments of the AGARD WG16CA Model," National Research Council, Inst. for Aerospace Research, IAR-AN-83, Ottawa, ON, Canada, Sept. 1995.

[24]Ericsson, L. E., "Unsteady Flow Separation on Slender Bodies at High Angles of Attack," *Journal of Spacecraft and Rockets*, Vol. 30, No. 6, 1993, pp. 689–695.

[25]Brandon, J. M., and Nguyen, L. T., "Experimental Study of Effects of Forebody Geometry on High Angle-of-Attack Stability," *Journal of Aircraft*, Vol. 25, No. 7, 1988, pp. 591–597.

[26]Ericsson, L. E., "Wing Rock Generated by Forebody Vortices," *Journal of Aircraft*, Vol. 20, No. 2, 1989, pp. 110–116.

[27]Ericsson, L. E., "Further Analysis of Wing Rock Generated by Forebody Vortices." *Journal of Aircraft*, Vol. 20, No. 12, 1989, pp. 1089–1104.

[28]Ericsson, L. E., and Beyers, M. E., "Conceptual Fluid/Motion Coupling in the Herbst Supermaneuver," *Journal of Aircraft*, Vol. 34, No. 3, 1997, pp. 271–277.